Think locally – linking structure, thermodynamics and transport in grossly non-stoichiometric compounds and solid solutions

Neil L. Allan,*[a] Svein Stølen[b] and Chris E. Mohn[b]

DOI: 10.1039/b806156d

We highlight the crucial influence of the *local* environment of individual cations or of oxygen vacancies on the structure and energetics of grossly non-stoichiometric compounds and solid solutions. Consideration of the average structure is not sufficient. In solid solutions non-ideality is strongly linked to the local environment, and our results question the use of models which assume entirely random distributions of particular ions or vacancies over particular lattice sites. We consider three examples: (i) the oxide $Ba_2In_2O_5$, representative of a family of oxygen-deficient perovskites; (ii) the superionic conductor α-CuI; (iii) the pyrope–grossular garnet solid solution. We emphasise the different insights gained into the solid state chemistry of these systems and the consequences for thermodynamic and transport properties.

Introduction

Many technologically important materials are both structurally and chemically complex and this complexity is often an essential ingredient in producing technologically valuable behaviour. But our understanding at the atomic level often remains severely limited. In particular, for grossly non-stoichiometric compounds, solid solutions, or disordered materials more generally, crystallographic techniques produce an 'average' structure based on partial occupancy of particular sites, but only yield very limited information about which local atomic arrangements or configurations give rise to or underlie this average. In the absence of more information and in simple statistical mechanical treatments such as mean field theory or regular solution models, it is usual to assume random distributions of cations or of vacancies consistent with this average. We shall see that such descriptions can fail spectacularly. For example, studies of the potential energy hypersurfaces in oxygen-deficient perovskites such as $Sr_2Fe_2O_5$ and $Ba_2In_2O_5$ reveal a strong energetic preference for only a small number of certain local structural entities. The average structure observed experimentally can then be interpreted as a spatial average of these local structures. This has major implications, not only for the thermodynamic properties but also for fast-ion transport and possible transport mechanisms. These must involve transitions between the basins corresponding to different local minima (basins) on the potential energy hypersurface and so must involve these structural entities.

Thus we are currently exploring the link between *local* structure and observed physical and materials behaviour,

[a]*School of Chemistry, University of Bristol, Cantock's Close, Bristol, BS8 1TS, UK*
[b]*Department of Chemistry and Centre for Materials Science and Nanotechnology, University of Oslo, Postbox 1033, Blindern, N-0315 Oslo, Norway*

Neil Allan

Neil Allan studied at Oxford University and received his D.Phil. from the same institution in 1986. He then worked in the Theory and Modelling Group at ICI New Science Group before moving to Bristol as a lecturer in 1989. He is currently Professor of Physical Chemistry at Bristol and his research interests include computational materials science and applications of theoretical chemistry to condensed phases and geochemical problems.

Svein Stølen received his Ph.D. from the University of Oslo in 1988. He is currently Professor at the Department of Chemistry at the same University. He is also affiliated with the Interdisciplinary Centre of Materials Science and Nanotechnology (SMN) and the FERMIO (Functional Energy Related Materials) Centre of excellence. His research ranges from experimental calorimetry and high pressure studies to computational chemistry and thermodynamic modelling.

Following his Ph.D. at the University of Oslo (2005) under the supervision of Svein Stølen, Chris Mohn worked as a postdoctoral fellow at the University of Bristol with Neil Allan. His fellowship now continues at the University of Montpellier with Walter Kob. His research involves the development and application of computational methods for modelling disordered materials.

including structure, thermodynamics, and transport. This project is very much still in its first stages, due to the difficulties associated with the modelling of solid solutions and grossly non-stoichiometric systems once one moves away from assuming ideal or regular solutions or defect distributions, or from traditional textbook 'mean-field' treatments that fail to allow for distinct local environments of the different species present. The challenge computationally is that of calculating the energies of a large number of possible atomic arrangements *while taking full account of the changes in local environment of each species from one arrangement to another*. This necessarily imposes an inevitable trade-off between the number of such arrangements and the computational cost. For problems such as those discussed in this paper we have developed a number of techniques,[1] ranging from new Monte Carlo simulations to Boltzmann (configurational) averaging of particular arrangements (configurations), calculating their internal energies and enthalpies using structure optimisation and either classical potential-based methods or periodic *ab initio* methods (principally density functional theory). The Boltzmann averaging thus follows the mapping of the individual local minima (basins) on the potential energy surface. Interbasin transitions (from one configuration to another) are assumed to be rare compared with intrabasin motion (vibration).

Where vibrational contributions and free energies are also required we have used a combination of lattice statics and quasi-harmonic lattice dynamics to calculate Gibbs energies of individual configurations, which are then Boltzmann-averaged. A useful alternative is often Monte Carlo simulations in the semi-grand canonical ensemble. We refer the reader to the references cited below for details of methodologies and their implementations.

In this paper we concentrate on the new chemical insights these are already providing for the materials chemist. We present three case studies which illustrate different aspects. In the first, oxygen-deficient perovskites illustrate a strong preference for a small number of particular metal coordination numbers and coordination geometries, even at elevated temperatures. Our second example is α-CuI. We shall see the importance of the flexibility of the iodide sublattice, which leads to a range in coordination numbers and local environments for both Cu (and I), rather than a preference for particular polyhedral coordinations. We discuss the implications of particular low-energy structures for the fast-ion conductivity of the perovskites and α-CuI. The final case study demonstrates some wider consequences of local order by examining how the take-up of trace elements by the pyrope–grossular garnet ($Mg_3Al_2Si_3O_{12}$–$Ca_3Al_2Si_3O_{12}$) solid solution is determined by the local environments of Mg^{2+} and Ca^{2+} in the solid solution. Particularly striking here is that key interactions involve atoms as far removed as third-nearest cation neighbours.

Grossly non-stoichiometric oxides – $Ba_2In_2O_5$ and related oxygen-deficient perovskites

$Ba_2In_2O_5$ adopts the brownmillerite-type structure, which consists of alternating two-dimensional layers of corner-shared InO_4 tetrahedra and corner-shared InO_6 octahedra. At low temperatures the InO_4 tetrahedra are regularly ordered with oxygen vacancies (vacant oxygen lattice sites) arranged in parallel chains as shown in Fig. 1a. There are three crystallographically distinct oxygen sites: O(1), which are in the equatorial planes of the octahedra, O(2) at the apices of the octahedra and O(3) those oxygens in tetrahedra not shared with octahedra. On heating brownmillerite-type oxides such as $Ba_2In_2O_5$, the entropy gain associated with disordering the oxygen sublattice often gives rise to order–disorder transitions, with an associated large jump in the ionic conductivity. The oxide ionic conductivity of $Ba_2In_2O_5$ increases more than ten-fold[2] at 1203 K, above which it is comparable to that of widely-used stabilized zirconia.

We have investigated the structural features of $Ba_2In_2O_5$ through studying the minima in the energy hypersurface of

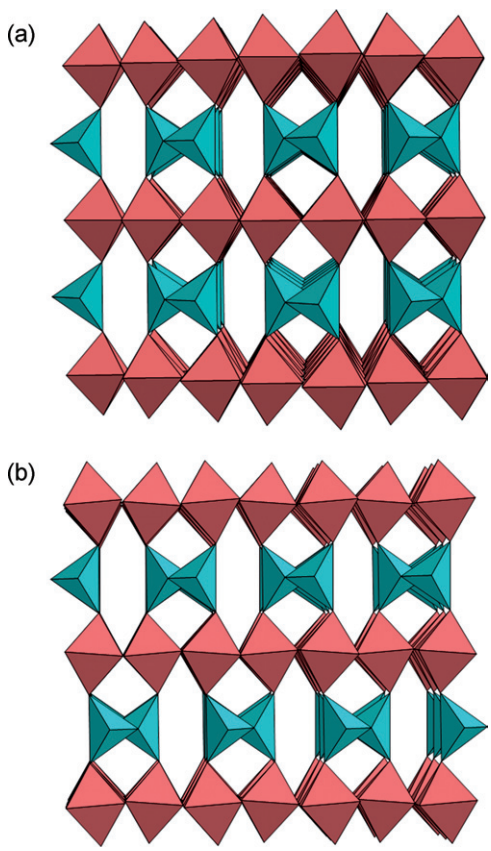

Fig. 1 Polyhedral representation of the two lowest-energy brownmillerite- related CNCs. The three different oxygen sites are marked. The two CNCs differ in the stacking of the tetrahedral layers: (a) the experimentally observed stacking where the vacancy channels are staggered along the *b*-axis; (b) the higher energy CNC where the vacancy channels are not staggered.

a 2×2×2 cell containing 36 atoms constructed by doubling a primitive cubic unit cell along each of the crystallographic directions. Initially 20 oxygen atoms are distributed over the 24 oxygen lattice sites of the ABO_3 supercell (giving 10 626 initial unrelaxed arrangements). A symmetry routine reduces this total to 78 initial unrelaxed crystallographically non-equivalent arrangements or configurations (CNCs). Structural optimizations with respect to all unit cell dimensions and atomic coordinates of each arrangement (CNC) were performed using density functional theory (DFT) within the generalized gradient approximation (GGA).[3] *No* symmetry constraints were imposed during the optimizations, which are accompanied by large relaxations and structural changes. The relative order of the energies of the CNCs changes after the relaxations. We stress that *full* structural optimizations of the atomic coordinates of each configuration are vital.

The final degeneracy *vs.* energy (*i.e.*, density of states) plot for the 2×2×2 cell is given in Fig. 2, where each symbol refers to a separate relaxed crystallographic non-equivalent configuration. *There are relatively few CNCs thermally accessible at most temperatures.* These are associated with different arrangements of tetrahedral InO_4 and octahedral InO_6 entities (which may be distorted to various extents) and to a much lesser extent square pyramidal InO_5. This is entirely consistent with the known solid state chemistry of In. The two lowest-energy CNCs both contain 50% octahedra and 50% tetrahedra. In the lowest energy CNC is the stacking along the *c*-axis is that experimentally observed (Fig. 1a). In the next lowest (Fig. 1b) the structure is very similar but the vacancy channels are not staggered. Fig. 3a shows the connectivity observed experimentally and obtained theoretically in both these two lowest-energy CNCs. In addition to brownmillerite-like configurations with different stacking sequences of the tetrahedral layer, some configurations with different types of connectivity within the tetrahedral layers are also low in energy. Four further connectivity patterns are given in Fig. 3 in order of increasing energy (a)–(d). These represent the eight different CNCs possible for our supercell with 50% tetrahedral and 50% octahedral indium. With increasing energy, CNCs have edge-sharing tetrahedra (Fig. 3b) and then zig-zag patterns of tetrahedra (Fig. 3c and d). None of the final optimised CNCs contained three or two fold In – all contained various combinations of four, five and six coordinated In with various degrees of local distortion.

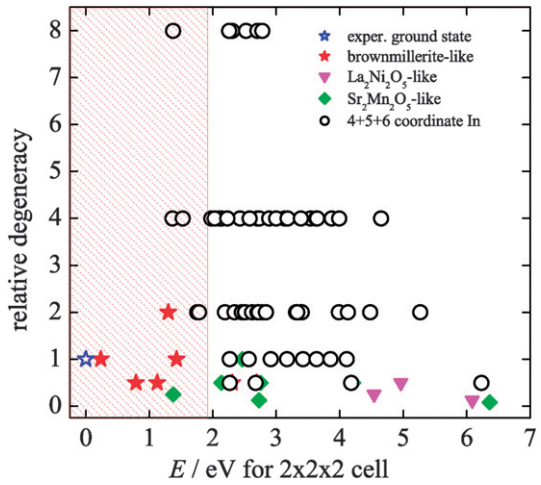

Fig. 2 Degeneracy–energy plot for the 2×2×2 cell of $Ba_2In_2O_5$. The shaded area identifies the energy region populated significantly at 2500 K.

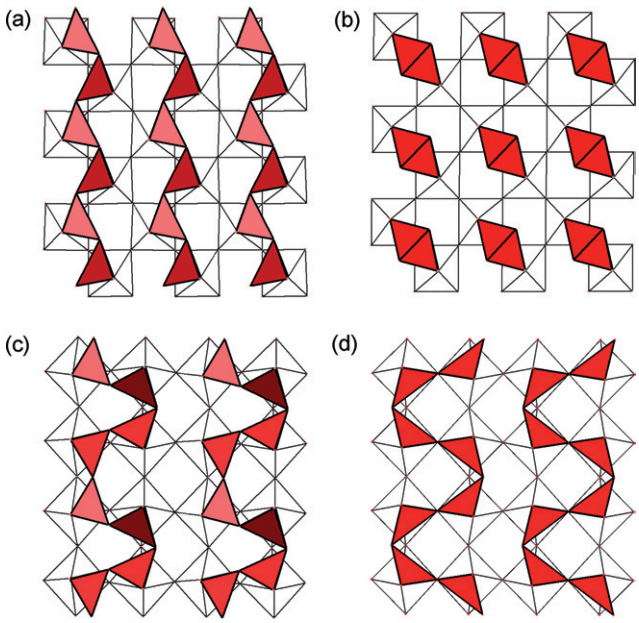

Fig. 3 Connectivity of the InO_4 tetrahedra in the *ac*-plane of different configurations containing 50% tetrahedrally and 50% octahedrally coordinated In in order of increasing (less negative) energy (a)–(d).

Boltzmann averaging of these results for individual configurations shows that O(1) and O(2) are fully populated to 1500 K, above which the occupancy of O(2) decreases significantly. O(1) is fully occupied to significantly higher temperatures, which supports the reported two-dimensional disorder and conductivity at intermediate temperatures. The number of possible sites available for the oxygen atoms is large, but strong structural correlations due to the preference for particular structural polyhedra imply that these will be far from randomly occupied. Thus in $Ba_2In_2O_5$ the distribution of oxygen vacancies is far from random and strongly non-ideal even in the high-temperature disordered phase, where locally the structure still consists of

alternating layers of InO_4 tetrahedra and InO_6 octahedra, but with a range of stacking sequences and tetrahedral connectivities. Our results are in line with the entropy of the disordered phase being considerably lower than the ideal value.[4] The existence of a number of different low-energy CNCs rationalises the frequent observation of incompletely ordered structures even at room temperature. At low temperatures the energy barriers from one minimum to another are thermally inaccessible. Complete long-range order is thus not easily achieved and frozen-in disorder results. The freezing of rapid oxygen ordering recently has been reported to give rise to glass-like transitions in perovskite-related oxides[5] and $ZrWMoO_8$.[6]

The energetic preference for certain structural entities also has implications for ionic transport due to restraints imposed by local symmetry. A conventional single vacancy jump mechanism requires different types of local short-range order that Fig. 2 shows are of high energy and thus must make a negligible contribution. Thus the ionic movement is highly restricted by the local symmetry. The transport *must* involve transformation of one thermally accessible local structure into another and consideration of the transport mechanism should involve consideration of the mechanisms of such transformations. Indeed, transition paths[7] connecting different low-energy CNCs characterized using the nudged-elastic-band method strongly indicate that correlated or concerted ion movements are important in fast oxide-ion conductors such as $Ba_2In_2O_5$. We have also extended these studies[8] to study the effect on the energy landscape shown in Fig. 2 of the incorporation of Sr and Ga, which substitute for Ba and In respectively, and so rationalised why Sr promotes fast-ion conduction, while it is inhibited by Ga. We have also compared[9] the energy landscapes of $Sr_2Fe_2O_5$ and $Ba_2In_2O_5$, both superionic conductors with the brownmillerite structure, with $Sr_2Mn_2O_5$ (square-pyramidal Mn(III)) and $La_2Ni_2O_5$ (square-planar Ni(III)), which are not. The possibility of many different oxygen orderings associated with a variety of low-energy connectivity schemes within tetrahedral layers such as in the brownmillerite structure appears to be a prerequisite for high ionic conductivity in perovskite-related $A_2B_2O_5$ oxides.

Using the same approach as ours, but with further *ab initio* molecular dynamics simulations, Hou *et al.*[10] have very recently demonstrated the correlated movement of the oxygen atoms in the important superionic conductor LAMOX and the significance in LAMOX in particular of certain four-fold or five-fold coordinated Mo cations. The importance of local atomic arrangements in LAMOX and the implications for the monoclinic-to-cubic phase transition have been elegantly probed experimentally by Malavasi *et al.*[11] Cooperative mechanisms of fast-ion conduction have also recently been established[12] in gallium-based oxides with tetrahedral moieties such as $LaBaGaO_4$, where a cooperative "cog-wheel" process operates, in which Ga_2O_7 units form and break up. Cooperative mechanisms are emerging as much more important in oxide-ion conduction than previously recognised.

α-CuI and superionic conduction

As our second example, we turn to another superionic conductor, α-CuI. Even though the structure has been studied for over 50 years, debate concerning the local coordinations of the coppers and the extent to which the positions of the coppers are correlated. For example, while reverse Monte Carlo analysis of neutron diffraction data[13] suggests the Cu–Cu distance can be as short as 1.9 Å, EXAFS indicates[14] a much higher value of 2.4 Å for the minimum Cu–Cu separation. There are also discrepancies between previous Born–Oppenheimer *ab initio*[15] and classical molecular dynamics.[16] Fig. 4a summarises the model for the average structure, while Fig. 4b shows the substantial variation in different Cu–Cu radial distribution functions available in the literature.

There must be a large variation in the local structure of α-CuI. *The variation in energy of the different local structural motifs cannot be deduced from the average structure*. Following the same approach as for $Ba_2In_2O_5$ in an earlier section, possible local arrangements of the Cu atoms in α-CuI have been considered in detail.[17] A set of initial arrangements are constructed, each configuration is fully optimized[17] using density functional theory[3] and ensemble averages calculated using Boltzmann (configurational) averaging.[1] To start with, 50 random symmetrically distinct arrangements of the 4 Cu atoms over the tetrahedral 8c, octahedral 4b and 'interstitial' 32f sites (*e.g.*, at (x,x,x) with $x = 0.375$) in a 8-atom unit cell (Fig. 4a) were optimised. The lowest energy arrangement corresponds to the zincblende structure, which is reasonable given it is structurally related to the γ-phase of CuI stable at low temperature. Only ≈20% of all arrangements investigated are accessible at 750 K. All these have only the 8c tetrahedral sites occupied. In agreement with neutron diffraction studies[13,18] but in disagreement with early EXAFS,[19] which suggested significant occupation of the octahedral site, all configurations where this site is occupied are high in energy and thermally inaccessible. To generate final results, a further set of optimisations of 25 randomly chosen configurations used a 64-ion cell and ignored this 4b site (see ref. 17 for full details).

The resulting *average* structure provides strong support for a recent X-ray diffraction study,[20] which showed 80% of the Cu atoms were randomly distributed at 8c sites and the remaining 20% over the 32f at 750 K. In particular configurations both Cu and I atoms are displaced appreciably from their *averaged* positions; both sublattices are very *flexible* and our calculations in the static limit reveal that the observed displacement of the Cu away from the 8c site[13] is due not only to vibration but also to the configurational disorder. While the peaks in our calculated pair distribution functions will in general be too narrow due to the neglect of lattice vibrations, the calculated Cu–Cu distance (Fig. 4c) is in very good agreement with the EXAFS data.[14] There is a prominent peak at ≈2.7 Å with a less intense broader peak at ≈4.3 Å. 2.7 Å is significantly less than the shortest 8c–8c separation (≈3 Å) if we had considered only the average structure and closer to an 8c–32f distance. The iodines are also appreciably displaced from their average positions. The association of peak maxima in a pair distribution function with a particular separation between two distinct positions of an *average* structure is highly questionable.

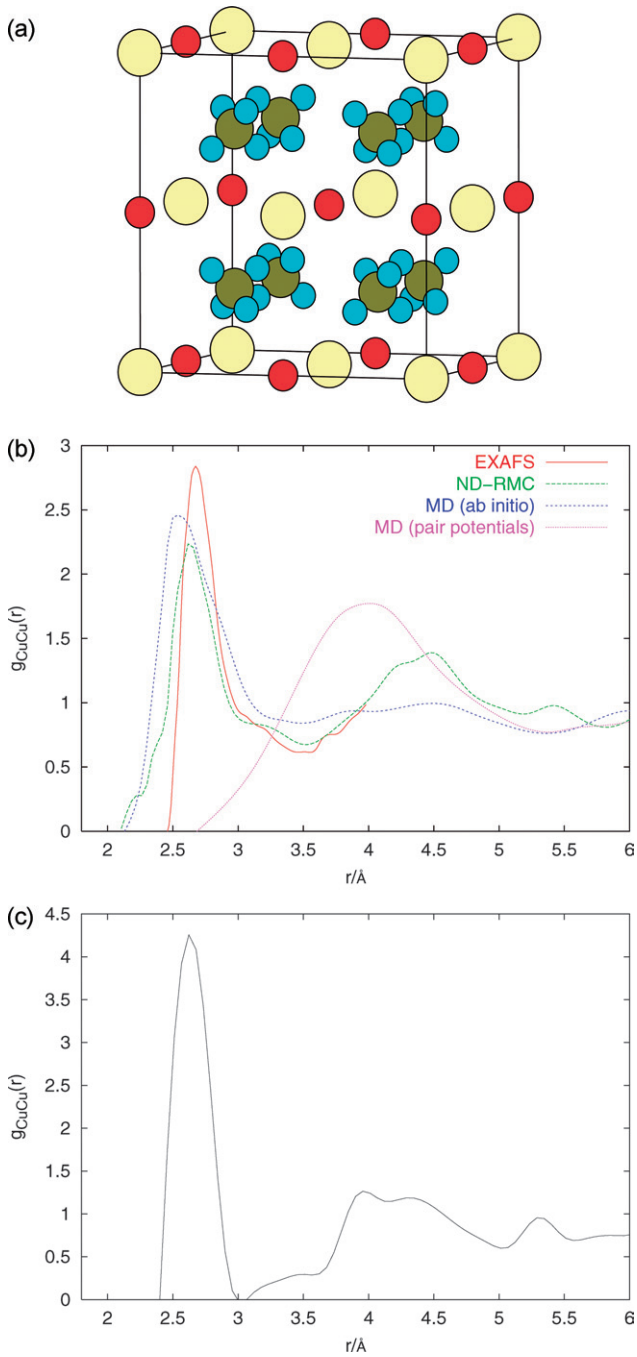

Fig. 4 (a) Possible crystallographic models which give rise to the observed average structure of α-CuI. Iodines are the large yellow spheres. Red, dark green and light grey are Cu atoms at octahedral 4b, tetrahedral 8c and 'interstitial' 32f sites respectively. The 32f sites lie at coordinates (x,x,x) *etc.* (x = 0.3) on the straight line connecting the tetrahedral 8c and the nearest octahedral 4b position. (b) Various different Cu–Cu pair distribution functions reported for α-CuI. EXAFS results[14] at 693 K are shown as thick full lines, neutron diffraction (reverse Monte Carlo) results[13] as thin full lines. The thick and thin dotted lines are results from *ab initio* molecular dynamics[15] and classical molecular dynamics simulations,[16] respectively. (c) Calculated Cu–Cu pair distribution function.

Turning to the local environment and the coordination of the Cu atoms, one third of the coppers are surrounded by three iodines and two thirds are surrounded by four. Once more this is consistent with the average structure, but the additional information available from examining the thermally accessible configurations is that many 4-fold coordinated coppers are located near the 32f and many three-fold coppers near 8c. The highly flexible I sublattice is the underlying cause, and we see yet again that the local structure may be very different from that of the average. This flexibility allows I atoms to respond readily to changes in the local environment as the Cu atoms diffuse, and a myriad of different diffusion trajectories is expected due to the large number of possible local environments possible both for I and Cu. A few representative examples are shown in Fig. 5.

Nevertheless, it is important to stress that the positions of the coppers are *strongly* correlated at short-range. A position adopted by a given Cu is strongly influenced by the positions of the neighbouring Cu atoms and this gives rise to particular peak positions in the RDFs and bond-angle distribution functions. These peaks can be at very different distances and angles from those expected from the average structure. The differences between the averaged structure and individual thermally accessible optimized arrangements of the superionic phase can be very striking, with some instantaneous structures displaying 'holes' and 'channels'. Further details are available in ref. 17.

New *ab initio* molecular dynamics calculations[21] are demonstrating the validity of this picture, with transitions between the low-energy configurations (the basins in the potential energy landscape) responsible for the fast-ion conduction. Average residence times are ≈8 ps, an order of magnitude higher than the vibrational period. In summary, α-CuI again shows the importance of considering the local structure and the details of the correlation between the atom positions, rather than just the average. The underlying structural chemistry of α-CuI is very different from that of the oxygen-deficient perovskites $Ba_2In_2O_5$ in that the flexibility of the structure and the variability in local coordination and environment gives rise to its exceptional transport properties, rather than a preference for particular polyhedral coordinations.

Solid solutions: non-ideality in garnets

Solid solutions are a further important general class of disordered systems which continue to present considerable

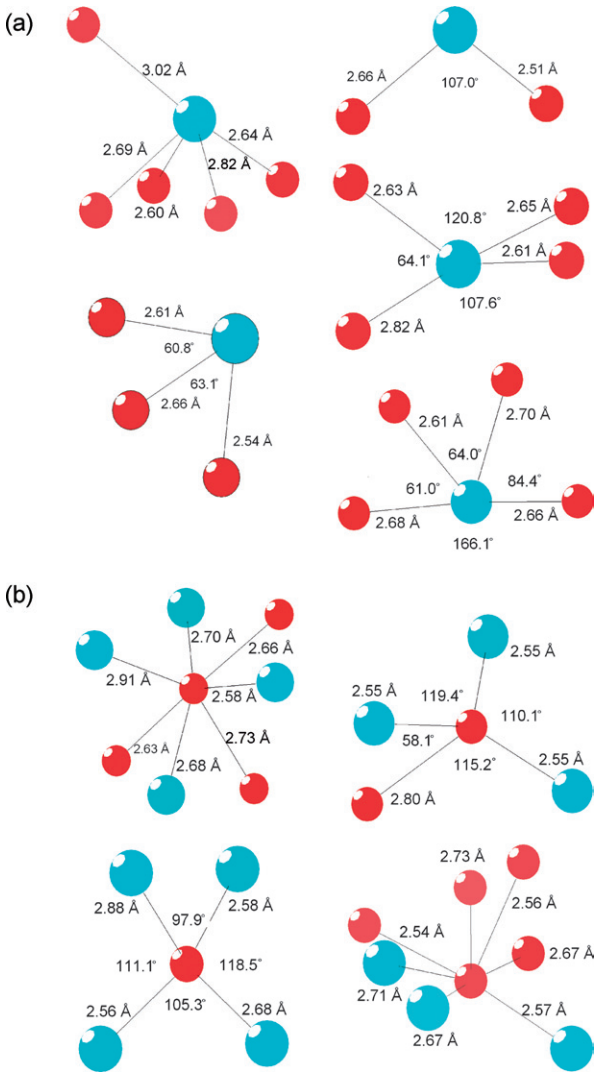

Fig. 5 Examples of local structural environments in thermally accessible configurations for α-CuI around (a) I (b) Cu. All atoms within 3 Å of the central atom are shown.

challenges. We have recently studied garnets ($X_3Y_2Z_3O_{12}$) including pyrope ($Mg_3Al_2Si_3O_{12}$) and grossular ($Ca_3Al_2Si_3O_{12}$) and the pyrope–grossular solid solution. This solution is highly non-ideal[22] and with the unusual feature that trace elements are considerably more soluble in the 50 : 50 solid solution than *either* of the end members.[23] As our last example, we show how the local order determines the properties of the solution and the implications of this for the incorporation of trace elements.

The non-ideality is clearly dependent on the rather complex crystal structure (Fig. 6). This is best viewed as a set of connected polyhedra: SiO_4 tetrahedra, AlO_6 octahedra and distorted XO_8 dodecahedra containing Mg or Ca cations which share edges with the tetrahedra and octahedra. The Mg/Ca cation–oxygen bonds are divided into two groups of four: cation–O1 and cation–O2. The latter are significantly longer by ≈0.15 Å. The Mg^{2+} cation is rarely found in 8-fold coordination due to its small size, which makes the local environment of the Mg cation in garnet interesting and unusual. The interconnected and relatively dense structure is such that the nature of the dodecahedral cations significantly influences the positions of the surrounding atoms.

A range of theoretical methods[24–27] have all been used to examine the X-site cation ordering and have revealed the unexpected importance of the 3rd nearest-neighbour (NN) cation interactions. Fig. 6b shows the 1st, 2nd and 3rd nearest neighbours of a given X-site cation and that the 3rd NN interaction involves two cations as far apart as ≈5.8 Å, separated by a SiO_4 tetrahedron. The edge-sharing SiO_4 tetrahedra and XO_8 dodecahedra form chains running along each unit cell vector. The simulations reveal a preference for a given cation to avoid an identical cation as its 3rd NN, resulting in low-temperature ordering. Experimentally, ^{29}Si NMR studies[28] have demonstrated a short-range cation ordering which decreases with increasing temperature.

We have examined the underlying reasons for this using *ab initio* (density functional theory[29]) and classical calculations of the end members pyrope and grossular and thirteen 50 : 50 pyrope–grossular configurations. Some optimizations were also performed on other configurations. Our calculations find that in pyrope the smaller Mg cation forms Mg–O bonds ≈5% shorter than the Ca–O bonds in grossular, accompanied by larger distortions of the framework. Fig. 7 plots the variation of the mean bond lengths X–O1 and X–O2 with solid-solution composition. The shorter X–O1 bonds (for *both* X = Mg and Ca) are rigid and maintain a virtually constant value for all compositions even in the dilute limit. There is a much larger variation for X–O2, again for both X = Mg and Ca. The longer X–O2 bond length varies almost linearly with solid solution composition.

We can now address the disagreement in the literature of the effect of the bulk composition of the solid solution on the local environment of the X-site cation, and specifically the variation in the X–O bond lengths. Considering *only* the four nearest oxygens as the *local environment*, we conclude that this is essentially independent of the bulk composition of the solid solution. EXAFS analysis at the Ca K-edge has suggested that the lengths of the Ca–O1 and Ca–O2 bonds converge with each other and the Mg–O2 bond length below ≈0.5 grossular mole fraction.[30] The picture that emerges from our first-principles calculations is quite different. We see a linear rather than non-linear variation in the X–O2 bond lengths, with no marked change at any particular composition. Due to the decrease of the Mg–O2 separation with increasing Mg content, the Mg–O2 and Ca–O1 bond lengths do get closer as the

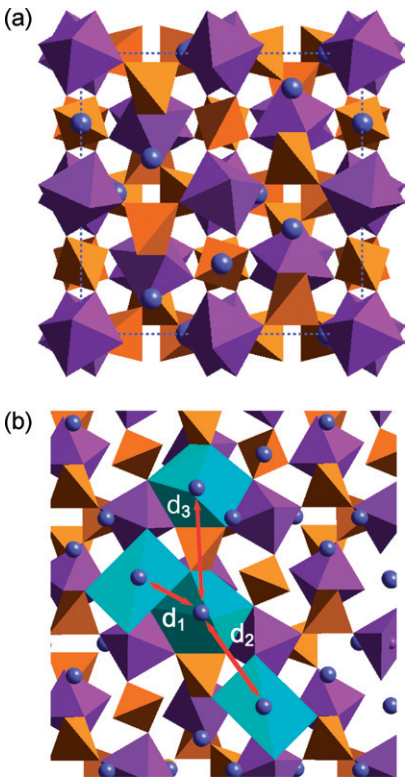

Fig. 6 (a) The garnet unit cell. SiO_4 tetrahedra are yellow, Al octahedra purple and cations (Ca and Mg) blue. Oxygen atoms are not shown. (b) Arrangement of the X-site cation–cation 1st, 2nd and 3rd nearest neighbours. Cations (blue atoms) are shown within their dodecahedra (light blue). The 1st, 2nd and 3rd nearest-neighbour (NN) distances between the cations are indicated as d_1 ($\approx$3.6 Å), d_2 ($\approx$5.4 Å) and d_3 ($\approx$5.8 Å) respectively. Note the arrangement of the SiO_4 tetrahedron which separates two 3rd NN cations.

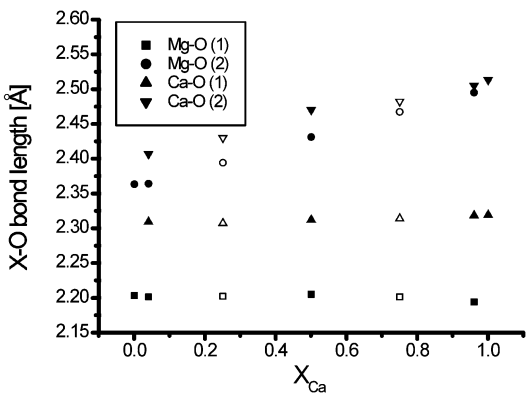

Fig. 7 Variation of the X–O (X = Mg, Ca) bond lengths with the mole fraction of grossular in the solid solution. Hollow points indicate the values where only two configurations have been used to generate the average distances. The filled points use either 13 configurations (for the $Gr_{50}Py_{50}$) or use the only unique configuration available.

magnesium mole fraction rises but at the 50 : 50 composition there is still an appreciable difference ($\approx$0.1 Å). A difference of 0.05 Å persists even in the dilute limit (Mg:Ca 96 : 4). Ca–O2 and Mg–O2 bond lengths are much closer than Ca–O1 and Mg–O1 at all compositions, differing at most by only $\approx$0.05 Å, but Ca–O2 remains slightly larger even in the dilute limit (Mg:Ca 4 : 96). The X–O1 bond length is independent of the bulk composition of the garnet solid solution and there is no convergence of either Ca–O1 or Ca–O2 bond lengths with Mg–O2. Further analysis of the EXAFS data is currently in progress to attempt to resolve these issues.

We have considered in detail[27] the local environment of the X cations and the structural changes this undergoes with different 3rd NN cations. The distortions of the SiO_4 tetrahedra associated with Mg–Mg 3rd NNs increase in the solid solution relative to those in pyrope itself (Fig. 8a). The local structural environment associated with Ca–Ca 3rd NNs in the 50 : 50 solid solution is quite different (Fig. 7b); overall these SiO_4 tetrahedra are much less distorted.

In general, the more Mg–Mg and Ca–Ca 3rd NNs present in a particular configuration the greater the energy of that configuration. The lowest energy configuration has no identical 3rd NN cations. The relative magnitudes of the *ab initio* energies after optimisation suggest that at ambient temperatures of 300 K only configurations with nearly all the cations arranged in Ca–Mg 3rd NN interactions are accessible and that complete cation randomisation occurs only above 1000 K. We can estimate the energies of the different configurations to estimate the mean energy associated with the equilibrium shown in eqn (1), in which a Ca–Ca 3rd NN unit and a Mg–Mg 3rd NN unit are replaced by two Ca–Mg 3rd NN combinations,

$$\text{Ca–Ca} + \text{Mg–Mg} \rightarrow 2\,\text{Ca–Mg} \qquad (1)$$

We estimate the energy of reaction (1) as -0.9 eV, using the energies of all the configurations.

At any composition the creation of an extra Ca–Ca 3rd NN interaction from a Ca–Mg pair necessarily involves also the formation of an Mg–Mg 3rd NN interaction. So the presence of the lower strain Ca–Ca 3rd NN necessarily results in the presence of the higher strain Mg–Mg 3rd NN, so a system with the greatest number of 'favourable' Ca–Ca interactions also possesses the greatest number of 'unfavourable' Mg–Mg interactions. Since reaction (1) is exothermic, energetically the distortion introduced by two Ca–Mg 3rd NNs is less than that for the combination of a Mg–Mg 3rd NN and a Ca–Ca 3rd NN. The preferential ordering seen in the pyrope–grossular garnets thus effectively results from the avoidance of small Mg cations together as 3rd NN pairs.

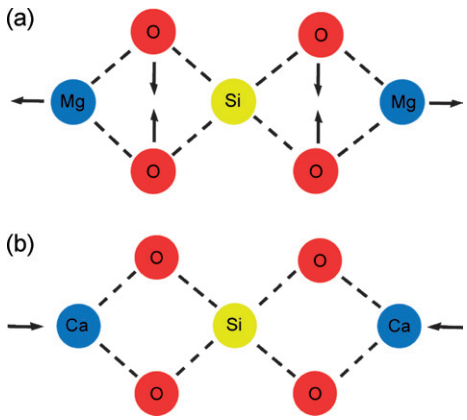

Fig. 8 Changes in the structure of the solid solution relative to the respective end members associated with different 3rd NN interactions for (a) Mg–Mg 3rd NNs and (b) Ca–Ca 3rd NNs.

The 3rd NN cation arrangement has dramatic consequences for incorporation of foreign cations (trace elements) in the solid solution.[31,32] Substitution patterns in ionic solids generally obey the long-established Goldschmidt's rules[33] which state that the two main principles governing substitution are size (ionic radius) mismatch and charge difference between substituent and host; the greater the similarity between the cations, the more readily substitution should take place. We have carried out classical simulations[31,32] of the energetics of solution reactions (2a) and (2b). Here divalent trace element cations substitute for Ca^{2+} or Mg^{2+} in the 50 : 50 garnet solid solution respectively, and:

$$JO + Ca_{1.5}Mg_{1.5}Al_2Si_3O_{12} \rightarrow JCa_{0.5}Mg_{1.5}Al_2Si_3O_{12} + CaO \quad (2a)$$

$$JO + Ca_{1.5}Mg_{1.5}Al_2Si_3O_{12} \rightarrow JCa_{0.5}Mg_{1.5}Al_2Si_3O_{12} + MgO \quad (2b)$$

where J is a divalent cation. These simulations established that *small* cations (*e.g.* Ni) substitute for a *large* Ca rather than the similarly sized Mg when both 3rd NNs are also Ca. Conversely, larger cations (*e.g.* Ca, Sr and Ba) substitute for Mg rather than Ca when both the 3rd NNs are Mg. The identity of the 3rd NN thus dictates the nature of substitution, and the avoidance of unfavourable local interactions dominates over the usual factors which lead to Goldschmidt's rules.

A key factor is removal or avoidance of higher strain Mg–Mg 3rd NN interactions. A large cation such as Ba will remove a Mg–Mg 3rd NN pair, creating a Mg–Ba 3rd NN combination which overall causes a smaller distortion of the garnet framework. High strain 3rd NN combinations are also avoided when small cations are introduced. Consider also the incorporation of Ni, which is similar in size to Mg. Ni substitutes preferentially for Ca in a Ca–Ca 3rd NN pair rather than for Ca in a Ca–Mg 3rd NN pair as the latter involves the formation of the unfavourable Ni–Mg combination. A similar argument involving the removal of Mg–Mg interactions explains why trace elements are more soluble in the solid solution than in the end members.[31]

Thus once more we see the crucial importance of the *local* environment of individual cations on the structure and energetics of the garnet solid solution. By performing a detailed structural analysis of particular optimised solid solution configurations, we see that the SiO_4 tetrahedra between a dodecahedrally coordinated cation and its 3rd NN are distorted, and that this distortion increases as the size of the cation or its 3rd NN decreases. There are major energetic as well as structural consequences.

Conclusions

We have highlighted the importance of considering the *local* structural environments that are energetically accessible for particular atoms in grossly non-stoichiometric compounds or solid solution. Consideration of the average structure alone is not sufficient, and can even be highly misleading.[34] In solid solutions non-ideality is also strongly linked to the local environment, and our results question the use of models which assume completely random distributions of ions or vacancies over particular lattice sites. We have considered three examples – the oxide $Ba_2In_2O_5$, representative of a family of oxygen deficient perovskites, the superionic conductor α-CuI and the pyrope–grossular garnet solid solution. There are important consequences for transport and correlated ion motion as well as thermodynamic properties and solid state reactions such as trace element (dopant) incorporation. With advances in computer power and *ab initio* computational methodologies, the long-term prospects of our work are a step change in our understanding of how the atomic-level behaviour governs the macroscopic physical and chemical behaviour, and of the importance of the local structure and environment in determining materials-related properties of technological interest.

Acknowledgements

Computational facilities for this work were made available by a number of EPSRC and HEFCE JREI grants to NLA, and by NOTUR grants to CEM and SS.

References

1 I. T. Todorov, N. L. Allan, M. Yu. Lavrentiev, C. L. Freeman, C. E. Mohn and J. A. Purton, *J. Phys.: Condens. Matter*, 2004, **16**, S2751.
2 J. B. Goodenough, J. E. Ruiz-Diaz and Y. S. Chen, *Solid State Ionics*, 1990, **40**, 21.
3 As implemented within the VASP program – see: G. Kresse and J. Hafner, *Phys. Rev. B*, 1993, **47**, 558; G. Kresse and J. Joubert, *Phys. Rev. B*, 1999, **59**, 1758.
4 For a discussion of this in brownmillerite $Sr_2Fe_2O_5$, see: E. Bakken, N. L. Allan, T. H. K. Barron, C. E. Mohn, I. T. Todorov and S. Stølen, *Phys. Chem. Chem. Phys.*, 2003, **5**, 2237.
5 A. I. Rykov, K. Nomura, T. Matsui and M. Seto, *Physica B*, 2004, **350**, 287.
6 S. Allen and J. S. O. Evans, *J. Mater. Chem.*, 2004, **14**, 151.
7 C. E. Mohn, N. L. Allan, C. L. Freeman, P. Ravindran and S. Stølen, *Phys. Chem. Chem. Phys.*, 2004, **6**, 3052.
8 C. E. Mohn, N. L. Allan and S. Stølen, *Solid State Ionics*, 2006, **177**, 223.
9 S. Stølen, C. E. Mohn, P. Ravindran and N. L. Allan, *J. Phys. Chem. B*, 2005, **109**, 12362.
10 C. J. Hou, Y. D. Li, P. J. Wang, C. S. Liu, X. P. Wang, Q. F. Fang and D. Y. Sun, *Phys. Rev. B*, 2007, **76**, 014104.

11 L. Malavasi, H. Kim, S. J. L. Billinge, T. Proffen, C. Tealdi and G. Flor, *J. Am. Chem. Soc.*, 2007, **129**, 6907.
12 E. Kendrick, J. Kendrick, K. S. Knight, M. S. Islam and P. R. Slater, *Nat. Mater.*, 2007, **6**, 871.
13 A. Chahid and R. L. McGreevy, *J. Phys.: Condens. Matter*, 1998, **10**, 2597.
14 A. Trapananti, A. D. Cicco and M. Minicucci, *Phys. Rev. B*, 2002, **66**, 014202.
15 F. Shimojo and M. Aniya, *J. Phys. Soc. Jpn.*, 2003, **72**, 2702.
16 X. J. M. Zheng-Johansson, I. Ebbsjö and R. L. McGreevy, *Solid State Ionics*, 1995, **82**, 115.
17 C. E. Mohn and S. Stølen, *J. Phys.: Condens. Matter*, 2007, **19**, 466208.
18 S. Hull, *Rep. Prog. Phys.*, 2004, **67**, 1233.
19 J. B. Boyce, T. M. Hayes and J. C. Mikkelsen Jr, *Phys. Rev. B*, 1981, **23**, 2876.
20 Y. Wasada, S. Kang, K. Sugiyama, M. Kimura and M. Saito, *J. Mater. Chem.*, 2002, **16**, 4393.
21 C. E. Mohn and S. Stølen, to be published.
22 C. A. Geiger, *Solid Solutions in Silicate and Oxide Systems (EMU Notes in Mineralogy, vol. 3)*, ed. C. A. Geiger, Eötvös University Press, Budapest, 2001, ch. 4, pp. 71–100.
23 W. van Westrenen, J. D. Blundy and B. J. Wood, *Am. Mineral.*, 1999, **84**, 838.
24 A. Bosenick, M. T. Dove and C. A. Geiger, *Phys. Chem. Miner.*, 2000, **27**, 398.
25 W. van Westrenen, N. L. Allan, J. D. Blundy, M. Yu. Lavrentiev, B. R. Lucas and J. A. Purton, *Phys. Chem. Miner.*, 2003, **30**, 217.
26 V. L. Vinograd, M. H. F. Sluiter, B. Winkler, A. Putnis, U. Hålenius, J. D. Gale and U. Becker, *Mineral. Mag.*, 2004, **68**, 101.
27 C. L. Freeman, N. L. Allan and W. van Westrenen, *Phys. Rev. B*, 2006, **74**, 134203.
28 A. Bosenick, C. A. Geiger and B. L. Phillips, *Am. Mineral.*, 1999, **84**, 1422.
29 The garnet *ab initio* calculations were carried out using the CASTEP code: M. C. Payne, M. P. Teter, D. C. Allan, T. A. Arias and J. D. Joannopoulos, 'CASTEP 4.2' (academic version, licensed under the UKCP-MSI Agreement, 1999), *Rev. Mod. Phys.*, 1992, **64**, All used the generalised gradient approach (GGA) with the Perdew–Wang exchange-correlation functional.
30 R. Oberti, S. Quartieri, M. C. Dalconi, F. Boscherini, G. Iezzi and M. Boiocchi, *Chem. Geol.*, 2006, **225**, 347.
31 W. van Westrenen, N. L. Allan, J. D. Blundy, M. Yu. Lavrentiev, B. R. Lucas and J. A. Purton, *Chem. Commun.*, 2003, 786.
32 C. L. Freeman, M. Yu. Lavrentiev, N. L. Allan, J. A. Purton and W. van Westrenen, *THEOCHEM*, 2005, **727**, 199.
33 V. M. Goldschmidt, *J. Chem. Soc. (London)*, 1937, **140**, 655.
34 For more failures of mean-field treatments see *e.g.*: J. A. Ball, M. Pirzada, R. W. Grimes, M. O. Zacate, D. W. Price and B. P. Uberuaga, *J. Phys.: Condens. Matter*, 2005, **17**, 7621.

